Int J Adv Manuf Technol (2017) 91:1809–1821
DOI 10.1007/s00170-016-9877-5

ORIGINAL ARTICLE

Optimization of blank shape and segmented variable blank holder force trajectories in deep drawing using sequential approximate optimization

Satoshi Kitayama[1] · **Hiroki Koyama**[2] · **Kiichiro Kawamoto**[3] · **Takuji Miyasaka**[3] · **Ken Yamamichi**[3] · **Takuya Noda**[3]

Received: 10 October 2016 / Accepted: 11 December 2016 / Published online: 23 December 2016

Abstract Blank holder force (BHF) is one of the important process parameters for successful sheet metal forming. Variable blank holder force (VBHF) that the BHF varies through the forming process is recognized as an advanced forming technology. It has also been reported that segmented VBHF (S-VBHF) is valid to a complex shape forming, but the optimal S-VBHF trajectories are rarely discussed and used. In addition to BHF, blank shape has an influence on the product quality. The blank shape minimizing the earing is still an important issue in sheet metal forming. Simultaneous optimization of both S-VBHF trajectories and blank shape is one of the crucial issues in industries. This paper proposes a method to simultaneously optimize both the segmented VBHF trajectories and the blank shape. Numerical simulation in sheet metal forming is so intensive that a sequential approximate optimization (SAO) using a radial basis function (RBF) network is adopted for the simultaneous design optimization. Based on the numerical result, the experiment using the AC servo press (H2W300, Komatsu Industry Corp.) that can conduct the optimal S-VBHF trajectories is carried out. It has been confirmed from the numerical and experimental result that the proposed approach is valid.

Keywords Deep drawing · Blank shape · Segmented variable blank holder force trajectories · Numerical simulation · Sequential approximate optimization

✉ Satoshi Kitayama
kitayama-s@se.kanazawa-u.ac.jp

Hiroki Koyama
hiroki6789@stu.kanazawa-u.ac.jp

Kiichiro Kawamoto
kiichirou_kawamoto@komatsu.co.jp

Takuji Miyasaka
takuji_miyasaka@komatsu.co.jp

Ken Yamamichi
ken_yamamichi@komatsu.co.jp

Takuya Noda
takuya_noda@komatsu.co.jp

[1] Kanazawa University, Kakuma-machi, Kanazawa 920-1192, Japan

[2] Graduate School of Natural Science and Technology, Kanazawa University, Kakuma-machi, Kanazawa 920-1192, Japan

[3] Komatsu Industries Corp, 1-1, Ono-machi-shinmachi, Kanazawa 920-0225, Japan

1 Introduction

Sheet metal forming is one of the important industrial technologies for producing light weight products with high productivity. There are many parameters for successful sheet forming such as lubrication, blank holder force (BHF), blank shape, and die geometry. Large blank shape generates large flange part called earing, which is wasted by trimmed off. Since blank shape directly affects the material cost, it is important to determine an optimal blank shape minimizing the earing. In addition to the blank shape, BHF has an influence on the product quality. High BHF leads to tearing, whereas low BHF results in wrinkling. The BHF for successful sheet forming is mainly determined by the trial and error method, and a constant BHF throughout the forming process is widely used.

Obermeyer and Majlessi suggested that variable blank holder force (VBHF) that controlled the BHF during forming process was one of the effective approaches for successful sheet forming [1]. It is very difficult and time-consuming to determine the VBHF trajectory for successful sheet forming through

experiments, and one of the effective approaches to determine the VBHF trajectory is to use numerical simulation. Let us briefly review several representative approaches to determine the VBHF trajectory in deep drawing. Hsu et al. developed a closed-loop type algorithm [2], in which both the punch force and the BHF were well controlled for successful sheet forming. The validity of the closed-loop type algorithm was examined through the experiment. Manabe et al. also proposed a closed-loop type algorithm to control punch speed and BHF [3], in which fuzzy controller was developed to control the BHF. In their system, the database that experimental results were stored was used to control the BHF, and the system depended on the database. Sheng et al. developed an algorithm for the VBHF using a proportional and integral (PI) controller [4]. By adjusting these gain coefficients, the VBHF trajectory was determined. Lo and Yang also developed an algorithm incorporating the proportional, integral, and derivative (PID) controller [5]. Similar approach incorporating the PID controller has been reported by Lin et al. [6]. Yagami et al. developed an algorithm to control the BHF eliminating wrinkling [7]. In their work, at first, a low BHF was applied. When the wrinkling was observed, a high BHF was used to eliminate the wrinkling. A low BHF was then applied again. By iterating this process, a successful forming was conducted. Kitayama et al. developed a simple closed-loop type algorithm for the VBHF considering the thickness deviation during forming process [8], and the validity of the proposed algorithm was confirmed through the experiments using an AC servo press (H1F150, Komatsu Industry Corp.). Unlike above papers, Wang et al. determined S-VBHF trajectories for a rectangle box deep drawing [9], in which their proposed algorithm using PID controller was extended to the S-VBHF trajectories. This paper suggests that S-VBHF trajectories are valid to more complex shape for successful sheet metal forming.

Due to the recent advance of design optimization technique coupled with machine learning, several papers using response surface method (RSM) have been published on the determination of VBHF trajectory in deep drawing. In particular, a sequential approximate optimization (SAO) that the response surface is repeatedly constructed and optimized by adding new sampling points has been recognized as an attractive approach. Jakumeit et al. determined an optimal VBHF trajectory by the SAO using the Kriging [10], in which four objective functions (wrinkling, tearing, maximum thinning, and springback) were minimized with the weighted sum. Wang et al. determined an optimal VBHF trajectory in deep drawing [11], in which the thickness deviation and the risk of both wrinkling and tearing were minimized. The forming limit diagram (FLD) was used to evaluate the risk of both wrinkling and tearing. Kitayama et al. determined the optimal VBHF trajectory of square cup deep drawing using the SAO with a radial basis function (RBF) network [12], in which the thickness deviation was minimized under the wrinkling and tearing constraints. The effect of VBHF trajectory is mainly discussed on springback reduction, and several approaches are well summarized in ref. [13]. Manoochehri and Kolahan adopted an artificial neural network (ANN) to predict the thinning of blank and optimized the process parameters such as die radius, punch radius, blank holder force, and frictional conditions by using the simulated annealing [25]. Then, they reported that the minimum thinning was well improved by using the optimal process parameters. Note that this paper does not adopt VBHF approach. Hosseini and Kadkhodayan introduced the concept of blank holder gap (BHG) profile [26], which controlled the distance between blank holder and die by the BHF. To determine the optimal BHG profile, neural network and simulated annealing were used. They confirmed through numerical simulation that the optimal BHG profile could produce the desired blank thickness. To control the BHG, VBHF approach was practically adopted. Meng et al. developed an active blank holder control system driven by a servo-motor [27], in which an elastomer was employed and the BHF could be controlled by changing the servo-motor speed actively. In addition, a fuzzy logic controller was developed to control the punch speed. Kitayama et al. identified the formability window of a difficult-to-draw material by using pulsating BHF and VBHF [28], in which the punch stroke was maximized under tearing and wrinkling constraints. In the pulsating BHF, the amplitude of the vibration, the frequency, the time, and the phase were optimized, whereas the VBHF trajectory was also optimized according to ref. [12]. Mostafapour et al. adopted pulsating blank holder force approach to control the material flow into die [29], in which the relationship between drawing depth and input variables (frequency of blank holder, amplitude of blank holder movement, and velocity of punch movement) was investigated. The results showed that the pulsating blank holder could increase significantly the limiting drawing ratio (LDR) of deep drawing process about 11.53%, comparison with static one. Ozturk et al. proposed a method to determine optimal profiles of hydraulic pressure and blank holder force [30], in which an adaptive finite element analysis method coupled with fuzzy control algorithm was developed. The optimal loading profiles could improve the LDR of AA 5754-O sheet material. This result indicates that VBHF trajectory will be useful for improving the LDR. One of our targets is to determine the VBHF trajectory in deep drawing, and the detailed approaches for springback reduction are then not described in this paper. Numerical simulation in deep drawing is generally so intensive that it is preferable to determine the VBHF trajectory with a small number of simulations. In general, closed-loop type algorithms for the VBHF trajectory require a large number of simulations, and the SAO approach can determine it with a small number of simulations. Then, we adopt the SAO approach.

Finally, let us briefly review blank shape optimization. Unlike research on VBHF trajectory, this research topic is one of the classical and important issues in deep drawing. In blank shape

optimization in deep drawing, it is important to determine an optimal blank shape minimizing earing. It is difficult to review all papers, and the representative ones are reviewed. Park et al. proposed a method for determining optimal blank shape using the geometrical shape error (GSE) [14], in which the finite element analysis (FEA) was repeatedly carried out until the GSE value became very small. The GSE is widely used for optimizing blank shape designs, and Wang et al. [15], Vafaeesefat [16], and Fazli and Arezoo [17] adopted it for determining the optimal blank shape design in deep drawing. Oliveira et al. indicated that GSE could not determine whether the finite element nodes of the blank were inside or outside the target contour [18]. They then proposed a target shape error (TSE), which quantified the magnitude of deviation of the flange contour from the required target contour. It is possible to determine an optimal blank shape minimizing the earing by using the GSE and TSE, but a closed-loop type algorithm should be developed. As described above, a closed-loop type algorithm for blank shape optimization also requires a large number of simulations. To determine an optimal blank shape with a small number of simulations, the SAO is adopted. Hino et al. used a RSM for determining the optimal blank shape in deep drawing [19], in which earing was minimized under two design constraints with a constant BHF. Naceur et al. used a moving least square approximation to determine an optimal blank shape [20], in which seven control points (nodes of the blank) were taken as the design variables. Liu et al. optimized a polygonal blank shape by using support vector regression (SVR) [21], in which the risk of tearing/wrinkling was approximated and five control points were taken as the design variables. Xiao et al. proposed a blank dimension method considering energy consumption, machine cost, and process time, in which a multi-objective design optimization using the non-dominated sorting genetic algorithm-II (NSGA-II) was solved [31]. They showed that the blank dimensions could be calculated from the cutting depth of minimum energy consumption and workpiece dimension. It is found from above brief review that the RSM approach to determine an optimal blank shape has recently been developed and recognized as one of the important methodologies in deep drawing.

The representative papers are listed in Table 1, from which we can find that the following issues should be resolved:

1. VBHF approach is still an important forming technology. Due to the recent advance of press machine such as servo press [22], the experiment using VBHF trajectory can be conducted. However, S-VBHF trajectories are rarely discussed and used. As described in ref. [9], the S-VBHF trajectories will be valid to more complex shape. It is important to propose a method to determine the optimal S-VBHF trajectories.
2. Blank shape also affects the product quality as well as the material cost. In deep drawing, it is important to determine an optimal blank shape minimizing earing. Numerical simulation in sheet metal forming is so intensive that the iterative approach using GSE and TSE is not preferable. In order to determine the optimal blank shape minimizing earing with a small number of simulations, the SAO is much suitable. We have developed the SAO system using the RBF network [23], and this is used as the design optimization tool.
3. It is found from Table 1 that optimization of VBHF trajectory and blank shape optimization are separately performed. Therefore, the blank shape is not taken into account in the papers on VBHF, whereas a constant BHF is used in the papers on blank shape. In addition, optimization of S-VBHF trajectories is rarely discussed and used. In this paper, the simultaneous design optimization of S-VBHF trajectories and blank shape using the SAO is performed. Based on the numerical result, the experiment using a servo press (H2W300, Komatsu Industry Corp.) is carried out in order to examine the validity of the proposed approach.

The rest of this paper is organized as follows: In the "Finite element analysis model and validation" section, the FEA model is described. In the "Simultaneous optimization of blank shape and S-VBHF trajectories" section, the simultaneous optimization of both segmented VBHF trajectories and blank shape is formulated. The numerical result is shown in the "Numerical and experimental result" section. In order to examine the validity of the proposed approach, the experiment is carried out.

2 Finite element analysis model and validation

2.1 Finite element analysis model

Our target product is a food-type tray, and the punch and the blank holders are shown in Fig. 1. Various blank holder forces (BHFs) can be applied to two blank holders. To develop the FEA model, the experiments using several constant BHFs were performed. However, in all experiments, the wrinkling and tearing can be observed. Then, by using these experimental results, the FEA model was developed.

The FEA model is shown in Fig. 2, in which the symbol *nelm* denotes the number of finite elements. For the symmetry, only a half model is used. The total stroke is set to 75 mm. It is clear from Fig. 2 that two blank holders (blank holder$_1$ and blank holder$_2$) are modeled, and two BHFs (BHF_1 and BHF_2) are applied to positive z-direction. The punch is fixed, and the die drops to the negative z-direction with 8700 mm/s. Note that the velocity of the die with 8700 mm/s is used to shorten the computational time (mass scaling is not used). We have already confirmed that there

Table 1 Representative papers of VBHF trajectory and blank shape optimization

Topic	Ref.	Author(s)	Year	Approach	Wrinkling/tearing criterion
VBHF	2	Hsu et al.	2000	Closed-loop	Not clearly described
	3	Manabe et al.	2002	Closed-loop using fuzzy controller	Wrinking: distance between die and blank holder Tearing: maximum thinning
	4	Sheng et al.	2004	Closed-loop using PI controller	Wrinking: distance between die and blank holder Tearing: maximum thinning
	5	Lo and Yang	2004	Closed-loop PID controller	Wrinking: distance between die and blank holder Tearing: maximum thinning
	6	Lin et al.	2007	Closed-loop using PID controller	Wrinking: distance between die and blank holder Tearing: maximum thinning
	7	Yagami et al.	2007	Closed-loop	Wrinking: distance between die and blank holder Tearing: not considered
	9	Wang et al.	2007	Closed-loop	Wrinking: distance between die and blank holder Tearing: maximum thinning
	8	Kitayama et al.	2010	Closed-loop	Wrinking: distance between die and blank holder Tearing: maximum thinning
	10	Jakumeit et al.	2005	SAO using Kriging	Wrinking: distance between die and blank holder Tearing: maximum thinning
	11	Wang et al.	2008	SAO using polynomial	FLD is used to evaluate the wrinkling and tearing
	12	Kitayama et al.	2012	SAO using RBF network	FLD is used to evaluate the wrinkling and tearing
	26	Hosseini and Kadkhodayan	2014	Neural network and simulated annealing	Wrinking: distance between die and blank holder Tearing: maximum thinning
	27	Meng et al.	2016	PID controller using fuzzy logic	Not discussed.
	28	Kitayama et al.	2016	SAO using RBF network	FLD is used to evaluate the wrinkling and tearing
Blank shape	14	Park et al.	1999	Closed-loop using GSE. A constant BHF is used.	After forming, FLD is used to check the wrinkling and tearing.
	15	Wang et al.	2009	Closed-loop using GSE. A constant BHF is used.	Not considered.
	16	Vafaeesefat	2011	Closed-loop using GSE. A constant BHF is used.	Not considered.
	17	Fazli and Arezoo	2012	Closed-loop using GSE. A constant BHF is used.	Not considered.
	18	Oliveira et al.	2009	Closed-loop using TSE. A constant BHF is used.	Not considered.
	19	Hino et al.	2006	RSM using quadratic polynomial (SAO is not used). A constant BHF is used.	Wrinkling criterion: not considered Tearing criterion: maximum thinning
	20	Naceur et al.	2008	RSM using quadratic polynomial	FLD is used to evaluate the wrinkling and tearing
	21	Liu et al.	2013	RSM using SVR (SAO is not used). A constant BHF is used.	FLD is used to evaluate the wrinkling and tearing
	31	Xiao et al.	2016	NSGA-II	Not considered.

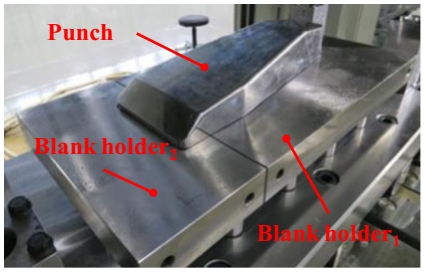

Fig. 1 Punch and blank holders

was no strain rate dependency during developing the FEA model. The rigid element is used to the punch, the die, and the blank holders. SUS304 is used as the blank, and the Belytschko-Tsay shell type element with nine integration points across the thickness is used for the blank in the numerical simulation. The friction coefficient and the penalty coefficient for contact in the interfaces (blank/punch, blank/blank holder, and blank/die) are set to 0.10 and 0.15, respectively. The material property is listed in Table 2. LS-DYNA, which is one of the dynamic explicit FEA codes, is used in the numerical simulation.

2.2 Validation of finite element analysis model

The validity of FEA model is examined. Both the dimensions and the forming limit diagram (FLD) are used to examine the validity of the FEA model. As shown in Fig. 3, five dimensions (A, B, C, D, and E) are selected to examine the dimension accuracy. The following three cases are tested for the validation of the FEA model: (case 1) $BHF_1 = BHF_2 = 40$ kN are applied. (Case 2) $BHF_1 = BHF_2 = 60$ kN are applied, and (case 3) $BHF_1 = BHF_2 = 120$ kN are applied. The numerical and experimental results are shown in Fig. 4 and Table 3. Note that the dimension errors are listed in Table 3. It is found from Fig. 4 that many finite elements are plotted in the wrinkling region with 40 kN and the wrinkling condition with 60 kN is improved. Finally, several finite elements are plotted in the tearing region with 120 kN. In particular, as shown in Fig. 4c, these plots in the numerical simulation agree well with the experimental result. In addition to the FLDs, as listed in Table 3, the dimension errors are small. It is confirmed from these results that the FEA model shown in Fig. 2 is valid.

Table 2 Material property of SUS304

Full blank size [mm] (Thickness × Length × Width)	0.80×650×380
Density: ρ [kg/mm3]	7.93×10^{-6}
Young's modulus: E [MPa]	2.13×10^{5}
Poisson's ratio: ν	0.26
Yield stress: σ_Y [MPa]	294
Normal anisotropy coefficient: r	1.00
Strain hardening coefficient: N	0.47
Friction coefficient	0.15
Penalty coefficient for contact	0.10
Number of integration points across the thickness (blank)	9

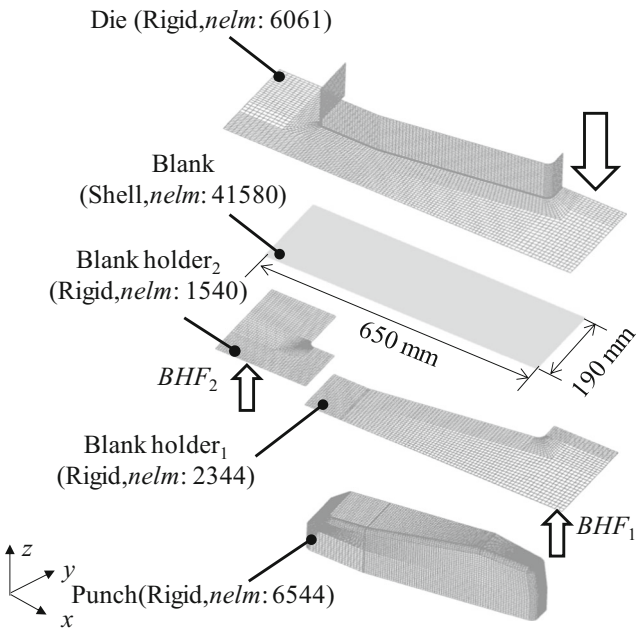

Fig. 2 Finite element analysis model

3 Simultaneous optimization of blank shape and S-VBHF trajectories

3.1 Objective function

The objective of this paper is to determine both the optimal blank shape minimizing the earing and the S-VBHF trajectories simultaneously.

First, let us explain about the objective function using Fig. 5, in which the solid line represents the exact shape and the dashed line the trimmed contour, respectively. As shown in Fig. 5, the trimmed contour is set to 15 mm from the exact shape. In this paper, the area above the

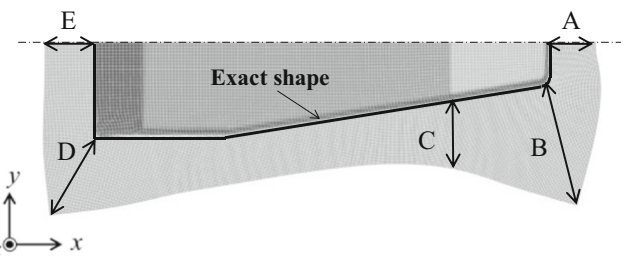

Fig. 3 Dimension accuracy

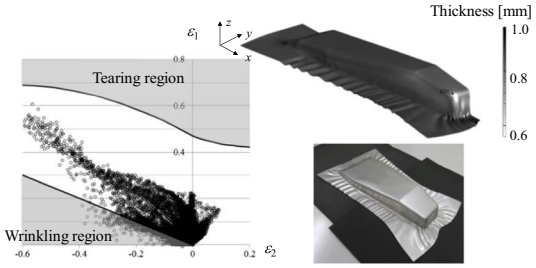

(a) Case1 (BHF_1=BHF_2=40 kN)

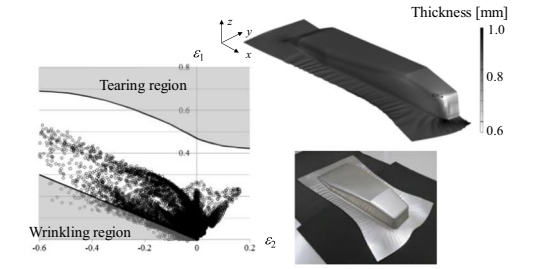

(b) Case2 (BHF_1=BHF_2=60 kN)

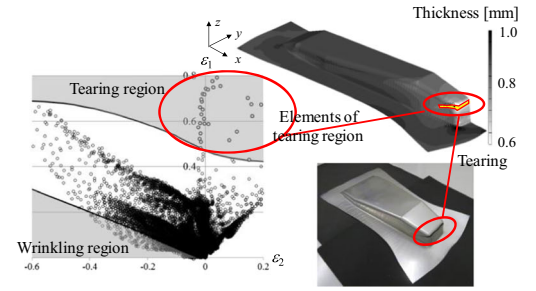

(c) Case3 (BHF_1=BHF_2=120 kN)

Fig. 4 FLD with numerical results and experimental results in all cases. **a** Case 1 (BHF_1 = BHF_2 = 40 kN). **b** Case 2 (BHF_1 = BHF_2 = 60 kN). **c** Case 3 (BHF_1 = BHF_2 = 120 kN)

trimmed contour is simply defined as the earing and is taken as the objective function to be minimized.

3.2 Design variables

Let us explain about the design variables. The design variables $\boldsymbol{x}$ consists of two parts: for the blank shape $\boldsymbol{x}_S$ and for the S-VBHF trajectories $\boldsymbol{x}_T$. The design variables can then be described as $\boldsymbol{x} = (\boldsymbol{x}_S, \boldsymbol{x}_T)^T$. First, let us explain about $\boldsymbol{x}_S$. For the blank shape, the six control nodes denoted by black circles in Fig. 6 are taken as the design variables.

Table 3 Dimension errors [%] in all cases

	A	B	C	D	E
Case 1	1.9	4.8	2.9	3.9	3.6
Case 2	0.9	5.2	4.5	1.0	5.5
Case3	0.3	0.7	3.0	1.8	0.0

Nodes 1 and 6 move along the horizontal line (x-axis), and nodes 3 and 4 move along the vertical line (y-axis), respectively. In addition, nodes 2 and 5 move along the vertex of the initial blank shape. Considering the blank cutting with a laser processing, these nodes are connected by straight line, and the optimal blank shape is then determined. The design variables for the blank shape are represented as follows:

$$\boldsymbol{x}_S = (s_1, s_2, \cdots, s_6) \tag{1}$$

Next, let us explain about $\boldsymbol{x}_T$. From the mechanical requirement to keep a balance between the blank holders, the following condition between the BHF_1 and BHF_2 is imposed:

$$BHF_1 = \alpha_{\max} \times BHF_2 \ \ (\text{or } BHF_2 = \alpha_{\max} \times BHF_1) \tag{2}$$

where $\alpha_{\max}(>1)$ is the coefficient which restricts the minimum and maximum BHF, and is a constant value. Equation (2) indicates that the minimum and maximum BHF completely depends on the other BHF. Concretely, let us consider a case where $\alpha_{\max}$ is set to 1.2. In this case, it is impossible to apply BHF_1 = 30 kN and BHF_2 = 70 kN. To keep the balance between the blank holders, the range of BHF_2 should be set from 25 kN(=30/1.2) to 42 kN under BHF_1 = 30 kN and vice versa (the range of BHF_1 should be set from 58.3(=70/1.2) to 84 kN under BHF_2 = 70 kN). Under this condition, a method to determine the S-VBHF trajectories is developed. To meet the mechanical requirement, we firstly consider the VBHF trajectory of blank holder$_1$. After that, we consider the VBHF trajectory of blank holder$_2$. First, as shown in Fig. 7, the total stroke is partitioned into M sub-stroke steps for the VBHF trajectory of the blank holder$_1$ in Fig. 2, and the BHFs of each sub-stroke step are then taken as the design variables. In addition, the sub-stroke steps denoted by $L_1, L_2, \cdots, L_{M-1}$ are taken as the design variables. In Fig. 7, $BHF_{1,k}$ ($k = 1, 2, \cdots, M$) indicates the BHF of the blank holder$_1$ at k-th sub-stroke step.

Next, let us consider the other VBHF trajectory ($BHF_{2,k}$, $k = 1, 2, \cdots, M$) of the blank holder$_2$. Equation (2) indicates that the VBHF trajectory of the blank holder$_2$ should be set within the gray area in Fig. 7. Then, the following equation is used to set the VBHF trajectory of the blank holder$_2$ within the gray area.

$$BHF_{2,k} = BHF_{1,k} \times \beta_k \ \ k = 1, 2, \cdots, M \tag{3}$$

where β_k is the design variables to meet the requirement of Eq. (2) and the range is given as follows:

$$\frac{1}{\alpha_{\max}} \le \beta_k \le \alpha_{\max} \quad k = 1, 2, \cdots, M \tag{4}$$

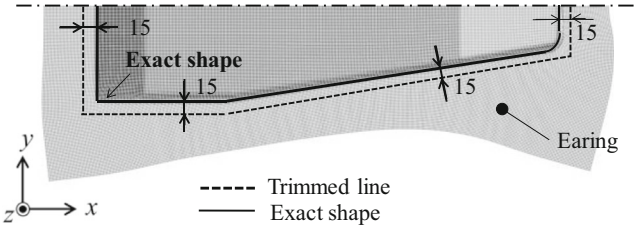

Fig. 5 Illustrative example of objective function

Note that β_k is unknown in advance and this is taken as the design variables. As the result, the design variables for the S-VBHF trajectories $\boldsymbol{x}_T$ are represented as follows:

$$\boldsymbol{x}_T = \Big(\underbrace{BHF_{1,1}, BHF_{1,2}, \cdots, BHF_{1,M}}_{\text{VBHF}_1}, \underbrace{\beta_1, \beta_2, \cdots, \beta_M}_{\text{VBHF}_2}, \underbrace{L_1, L_2, \cdots, L_{M-1}}_{\text{Stroke-steps}}\Big)^T \quad (5)$$

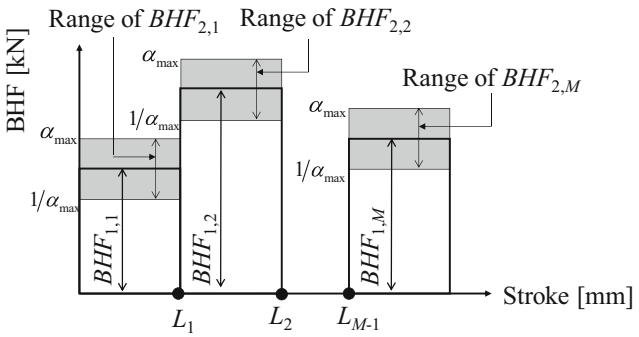

Fig. 7 Design variables for S-VBHF trajectories

Totally, the design variables $\boldsymbol{x}$ can be given as follow:

$$\begin{aligned}\boldsymbol{x} &= (\boldsymbol{x}_S, \boldsymbol{x}_T)^T \\ &= \Big(\underbrace{s_1, s_2, \cdots, s_6}_{\text{Blank shape}}, \underbrace{BHF_{1,1}, BHF_{1,2}, \cdots, BHF_{1,M}}_{\text{VBHF}_1}, \underbrace{\beta_1, \beta_2, \cdots, \beta_M}_{\text{VBHF}_2}, \underbrace{L_1, L_2, \cdots, L_{M-1}}_{\text{Stroke-steps}}\Big)^T\end{aligned} \quad (6)$$

3.3 Design constraints

Finally, let us describe the design constraints. Tearing and wrinkling are major defects, and they should be strongly avoided for successful forming. They are then considered as the design constraints. The FLD is used to numerically evaluate the tearing ($g_1(\boldsymbol{x})$) and wrinkling ($g_2(\boldsymbol{x})$). The strains in the formed finite element are plotted in the FLD, as shown in Fig. 8. The forming limit curve (FLC) in Fig. 8 was defined in the principal plane of logarithmic strains proposed by Hillman and Kubli [24].

$$\varepsilon_1 = \varphi_T(\varepsilon_2) \quad \varepsilon_1 = \varphi_W(\varepsilon_2) \quad (7)$$

where φ_T is the FLC that controls tearing, and φ_W is the FLC that controls wrinkling. Then, the following safety FLC is defined:

$$\left.\begin{aligned}\theta_T(\varepsilon_2) &= (1-s)\varphi_T(\varepsilon_2) \\ \theta_W(\varepsilon_2) &= (1+s)\varphi_W(\varepsilon_2)\end{aligned}\right\} \quad (8)$$

where s represents the safety tolerance, and is defined by the engineers (in this paper, s is set to 0.1). If an element comes to or lies above FLC, it is assumed that a risk of tearing can be observed. Similarly, a risk of wrinkling can be assumed if an element lies in the wrinkling region. By using the following equations, the tearing and wrinkling are numerically evaluated:

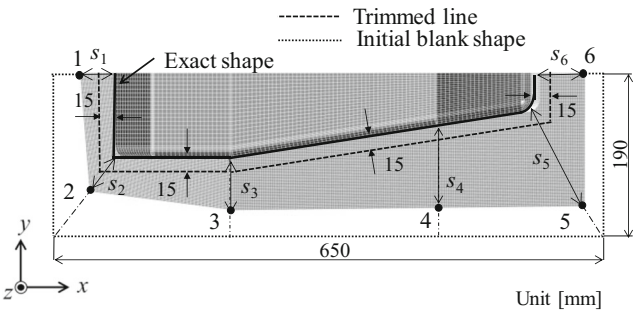

Fig. 6 Design variables for blank shape

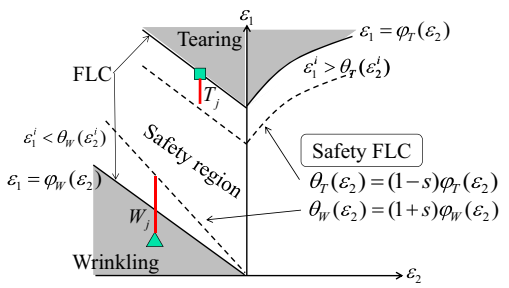

Fig. 8 Forming limit diagram for evaluating tearing and wrinkling

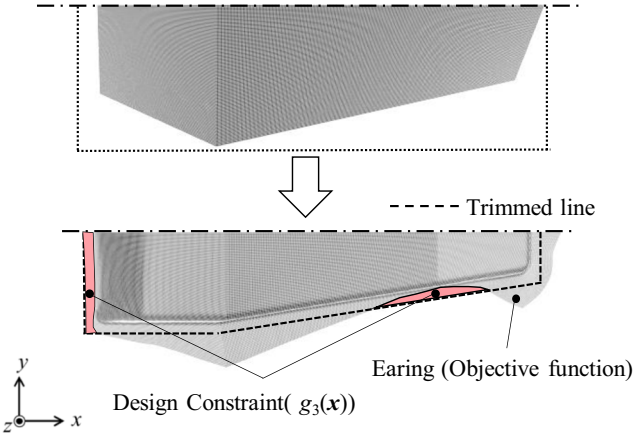

Fig. 9 Illustrative example of area below trimmed contour

For tearing

$$g_1(\boldsymbol{x}) = \left(\sum_{j=1}^{\text{nelm}} T_j\right)^{1/p} \quad \begin{cases} T_j = \left(\varepsilon_1^j - \theta_T\left(\varepsilon_2^j\right)\right)^p & \varepsilon_1^j > \theta_T\left(\varepsilon_2^j\right) \\ T_j = 0 & \text{otherwise} \end{cases} \tag{9}$$

For wrinkling

$$g_2(\boldsymbol{x}) = \left(\sum_{j=1}^{\text{nelm}} W_j\right)^{1/p} \quad \begin{cases} W_j = \left(\theta_W\left(\varepsilon_2^j\right) - \varepsilon_1^j\right)^p & \varepsilon_1^j < \theta_W\left(\varepsilon_2^j\right) \\ W_j = 0 & \text{otherwise} \end{cases} \tag{10}$$

Based on the literature [11, 12], p is set to 4. Also, *nelm* represents the number of finite elements of the blank.

Next, let us explain about the third design constraint $g_3(\boldsymbol{x})$. As shown in Fig. 9, the area below the trimmed contour is generated with undesirable blank shape. It is strongly required that the area below the trimmed line should not be generated. To meet this design requirement, the area below the trimmed contour is directly taken as the third design constraint $g_3(\boldsymbol{x})$. Note that the area above the trimmed contour is always evaluated and taken as the objective function. When the area below the trimmed contour is not generated, zero is assigned to $g_3(\boldsymbol{x})$.

3.4 Procedure for simultaneous optimization using sequential approximate optimization

The procedure for the simultaneous design optimization of blank shape and S-VBHF trajectories is described in this section. To perform the simultaneous design optimization, the SAO using the RBF network is used. The detailed procedure of the SAO using the RBF network is described in Appendix, and only the procedure is described.

Step 0: Assume that the number of sampling points is m. The initial sampling points are determined by using the Latin hypercube design (LHD).

Step 1: Numerical simulation is carried out at sampling points, and the objective function (the area above the trimmed contour) and the design constraints (tearing: $g_1(\boldsymbol{x})$, wrinkling: $g_2(\boldsymbol{x})$, and the area below the trimmed contour: $g_3(\boldsymbol{x})$) are evaluated. Then, the response surface of the objective function and the design constraints is constructed and optimized.

Step 2: If the terminal criterion is satisfied, the SAO algorithm using the RBF network will be terminated. Otherwise, to improve the local accuracy, the optimal solution is added. At this point, the total number of sampling points is updated as $m := m + 1$.

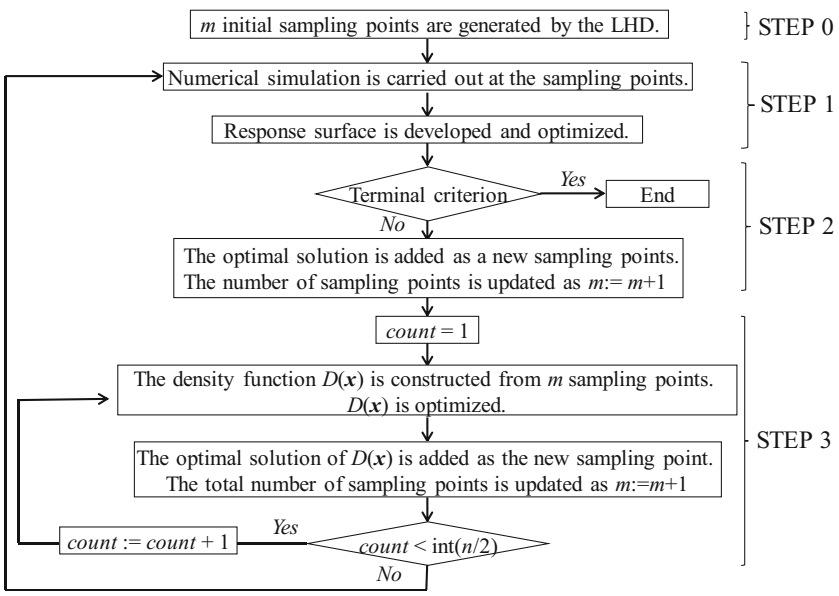

Fig. 10 Procedure of SAO using RBF network

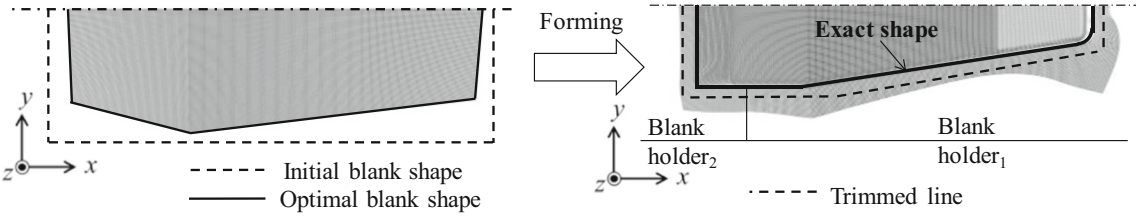

Fig. 11 Optimal blank shape and deformed shape in numerical result

Step 3: The density function to explore an unexplored region is constructed and optimized. The optimum of the density function is taken as the new sampling point, and the number of sampling points is updated as shown in Fig. 10, where the parameter *count* is introduced in this phase. This parameter controls the number of sampling points that can be obtained by the density function. Thus, in the proposed algorithm, the number of sampling points by the density function varies according to the number of design variables. If the parameter *count* is less than int(n/2), this parameter is increased as $count = count + 1$. The terminal criterion in this stage is given by int(n/2), where int() represents the rounding-off. By the iterative use of density function, it is expected to distribute the sampling points uniformly. As the result, global approximation can be achieved. The detailed procedure to construct the density function is described in Appendix. Then, the SAO algorithm will return to step 1.

The procedure is summarized in Fig. 10, where the differential evolution (DE) is used as the optimizer.

4 Numerical and experimental result

First, the numerical result is reported. Based on the numerical result, the experiment using AC servo press (H2W300, Komatsu Industry Corp.) is carried out. The total stroke is partitioned into three sub-stroke steps, and the lower and upper bounds of the design variables are set as follows:

$$\left.\begin{array}{lll} 19[mm]\le s_1\le 45[mm] & 30[mm]\le s_2\le 60[mm] & 48[mm]\le s_3\le 70[mm] \\ 75[mm]\le s_4\le 120[mm] & 48[mm]\le s_5\le 90[mm] & 45[mm]\le s_6\le 63.5[mm] \end{array}\right\} \quad (11)$$

$$\left.\begin{array}{ll} 10[mm]\le L_1\le 45[mm] & 50[mm]\le L_2\le 73[mm] \\ 40[kN]\le BHF_{1,k}\le 140[kN] & \frac{1}{1.3}\le\beta_k\le 1.3 \quad k=1,2,3 \end{array}\right\} \quad (12)$$

Equation (10) represents the lower and upper bounds for the blank shape, and Eq. (11) represents the one for the S-VBHF trajectories. Note that $\alpha_{\max}$ in Eq. (2) is set to 1.3 for the mechanical requirement of AC servo press. In this paper, the error at the optimal solution is adopted as the terminal criterion, which is set to 5.0%.

One single simulation in LS-DYNA costs about 45 min using a Core i7-4770 CPU 3.4GHz with four cores. Thirty-five initial sampling points are generated by the LHD, and the SAO using the RBF network is performed. Finally, we could obtain the optimal solution with 63 sampling points. In other words, in order to obtain the optimal solution, 63 simulations are required. The optimal blank shape and S-VBHF trajectories are shown in Figs. 11 and 12. The FLD at the optimal solution is also shown in Fig. 13, from which it is found that no tearing and wrinkling can be observed. It is found from Fig. 12 that S-VBHF trajectories cross through the

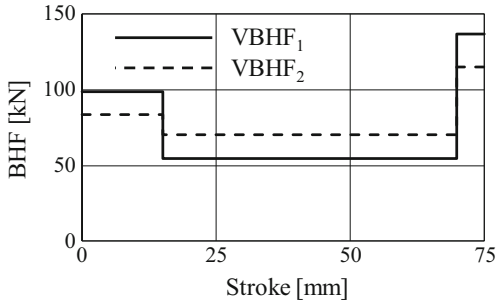

Fig. 12 Optimal S-VBHF trajectories in numerical result

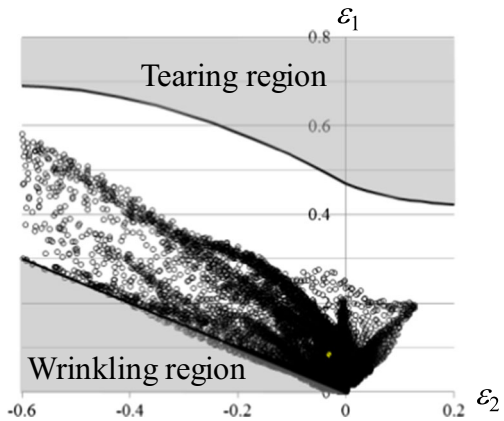

Fig. 13 Forming limit diagram at optimal solution

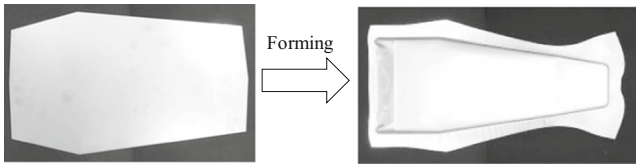

Fig. 14 Optimal blank shape and deformed shape in experiment

Table 4 Dimension errors

	A	B	C	D	E
Numerical simulation [mm]	20.7	69.2	22.7	36.1	20.7
Experiment [mm]	22.4	71.6	20.7	31.7	19
Error [%]	7.6	3.4	9.7	13.9	8.9

forming. At the early stage of the forming, the high BHF is applied to the blank holder$_1$ for compressing the wrinkling. On the other hand, the low BHF is applied to the blank holder$_2$ for flowing the blank into the die. At the early stage, the high BHF is applied to the blank holder$_1$, compared with the one of blank holder$_2$. This indicates that the risk of wrinkling of blank holder$_1$ is higher than that of blank holder$_2$. To suppress the wrinkling of blank holder$_1$, the high BHF is applied. Let us move on to the middle stage. At this stage, in order to avoid the tearing, both BHFs decrease. It will be useful to apply the low BHFs for avoiding the tearing, but the low BHFs will cause the wrinkling. Note that the high BHF of blank holder$_2$ is applied at this stage. In contrast to the early stage, the risk of wrinkling of blank holder$_2$ will be higher than that of blank holder$_1$. Then, the high BHF is applied to the blank holder$_2$. Finally, let us consider the final stage. At the final stage, both BHFs increase again for avoiding the wrinkling. The risk of wrinkling will be high at this stage, then both BHFs are high. In contrast to the middle stage, the high BHF of blank holder$_1$ is applied, compared with the one of blank holder$_2$. This indicates that the risk of wrinkling of blank holder$_1$ is higher than that of blank holder$_2$. As the result, the high BHF is applied to the blank holder$_1$ again. The optimal S-VBHF trajectories can well control the material flow into the die, and consequently, the successful sheet forming can be achieved.

Based on the numerical result, the experiment using AC servo press (H2W300, Komatsu Industries, Corp.) is carried out. The average die speed in the experiment is approximately 88 mm/s. The optimal blank shape and the deformed shape in the experiment are shown in Fig. 14. Figure 15 shows the optimal S-VBHF trajectories in the experiment, where the dashed line denotes the numerical result and the solid one the experimental result. It is clear from the experimental result that the successful sheet metal forming is performed. In addition, the AC servo press shows the high performance for the S-VBHF trajectories. The dimension errors shown in Fig. 3 are listed in Table 4, from which the dimension errors are much small.

Readers may consider that this product can produce a VBHF trajectory without S-VBHF trajectories. Then, we examined whether the successful sheet forming could be achieved or not without S-VBHF trajectories. By setting $BHF_1 = BHF_2$, the simultaneous optimization of blank shape and VBHF trajectory was performed. Unfortunately, no feasible solution could be obtained. In other words, the optimal solution satisfying all design constraints could not be obtained. Concretely, the wrinkling design constraint was always violated. To confirm this result, the experiment is carried out. The VBHF trajectory and the experimental result are shown in Figs. 16 and 17, from which it is found that the wrinkling can be observed on the flange. Consequently, it is confirmed that the proposed approach is valid for the successful sheet forming.

5 Conclusion

1. In this paper, simultaneous optimization of blank shape and segmented variable blank holder force

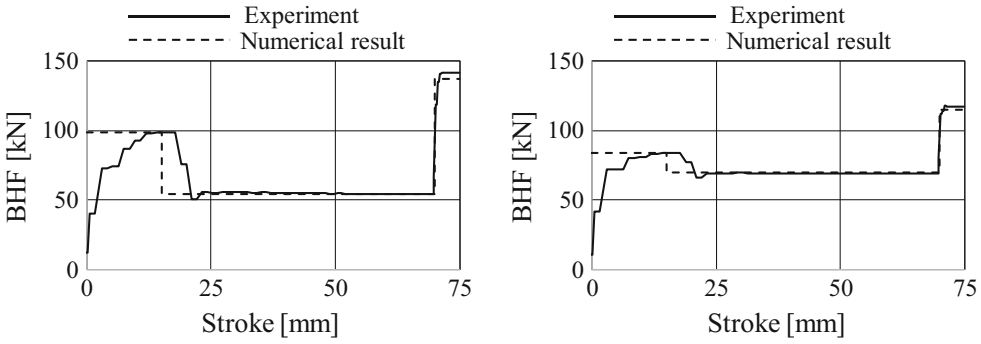

Fig. 15 Optimal S-VBHF trajectories in experiment

(a) VBHF trajectory of blank holder$_1$

(a) VBHF trajectory of blank holder$_2$

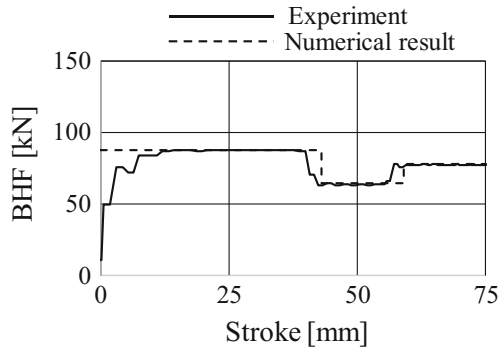

Fig. 16 VBHF trajectory in the experiment

trajectories is performed. To perform the simultaneous optimization, the area above the trimmed line is taken as the objective function to be minimized. The wrinkling and tearing which are numerically evaluated by the FLD are handled as the design constraints. In addition, to avoid undesirable product, the area below the trimmed line is also taken as the design constraint.

2. Based on the experimental results, the FEA model is developed. The validity of the FEA model is fully examined.
3. From the mechanical requirement to keep a balance between the blank holders, the minimum and maximum BHF completely depends on the other BHF. A method to meet this requirement is proposed for the segmented variable blank holder force trajectories.
4. Numerical simulation in the sheet metal forming is so intensive that the sequential approximate optimization using the radial basis function network is adopted for the simultaneous design optimization. It is found from the numerical result that the optimal S-VBHF trajectories cross through the forming. The optimal S-VBHF trajectories can well control the material flow into the die, and consequently, the successful sheet forming can be achieved.
5. Based on the numerical result, the experiment using the servo press (H2W300, Komatsu Industry Corp.) that can conduct the segmented variable blank holder force trajectories is carried out. Through the numerical and experimental result, the validity of the proposed approach is confirmed.

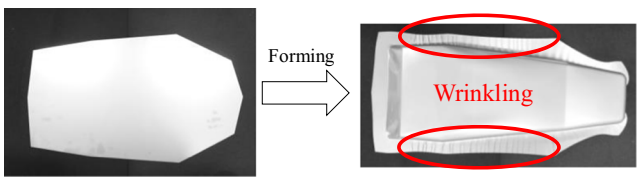

Fig. 17 Experimental result using VBHF approach

Appendix

Sequential approximate optimization (SAO) using a radial basis function (RBF) network is described in this appendix. In particular, the RBF network is used throughout the SAO procedure. The RBF network and the density function are briefly described.

Radial basis function network

The RBF network is a three-layer feed-forward network. The response surface using the RBF network is given by

$$y(\boldsymbol{x}) = \sum_{j=1}^{m} w_j K(\boldsymbol{x}, \boldsymbol{x}_j) \tag{A1}$$

where m denotes the number of sampling points, $K(\boldsymbol{x}, \boldsymbol{x}_j)$ is the j-th basis function, and w_j denotes the weight of the j-th basis function. The following Gaussian kernel is generally used as the basis function:

$$K(\boldsymbol{x}, \boldsymbol{x}_j) = \exp\left(-\frac{(\boldsymbol{x}-\boldsymbol{x}_j)^T(\boldsymbol{x}-\boldsymbol{x}_j)}{r_j^2}\right) \tag{A2}$$

In Eq. (A2), $\boldsymbol{x}_j$ represents the j-th sampling point, and r_j is the width of the j-th basis function. The response y_j is calculated at the sampling point $\boldsymbol{x}_j$. The learning of RBF network is usually accomplished by solving

$$E = \sum_{j=1}^{m} \left(y_j - y(\boldsymbol{x}_j)\right)^2 + \sum_{j=1}^{m} \lambda_j w_j^2 \rightarrow \min \tag{A3}$$

where the second term is introduced for the purpose of the regularization. It is recommended that λ_j in Eq. (A3) is sufficient small value (e.g., $\lambda_j = 1.0 \times 10^{-2}$). The necessary condition of Eq. (A3) result in the following equation.

$$\boldsymbol{w} = \left(\boldsymbol{H}^T\boldsymbol{H} + \boldsymbol{\Lambda}\right)^{-1}\boldsymbol{H}^T\boldsymbol{y} \tag{A4}$$

where $\boldsymbol{H}$, $\boldsymbol{\Lambda}$, and $\boldsymbol{y}$ are given as follows:

$$\boldsymbol{H} = \begin{bmatrix} K(\boldsymbol{x_1}, \boldsymbol{x_1}) & K(\boldsymbol{x_1}, \boldsymbol{x_2}) & \cdots & K(\boldsymbol{x_1}, \boldsymbol{x}_m) \\ K(\boldsymbol{x_2}, \boldsymbol{x_1}) & K(\boldsymbol{x_2}, \boldsymbol{x_2}) & \cdots & K(\boldsymbol{x_2}, \boldsymbol{x}_m) \\ \vdots & \vdots & \ddots & \vdots \\ K(\boldsymbol{x}_m, \boldsymbol{x_1}) & K(\boldsymbol{x}_m, \boldsymbol{x_2}) & \cdots & K(\boldsymbol{x}_m, \boldsymbol{x}_m) \end{bmatrix} \tag{A5}$$

$$\boldsymbol{\Lambda} = \begin{bmatrix} \lambda_1 & 0 & \cdots & 0 \\ 0 & \lambda_2 & \cdots & 0 \\ \vdots & \vdots & \ddots & \vdots \\ 0 & 0 & 0 & \lambda_m \end{bmatrix} \tag{A6}$$

$$\boldsymbol{y} = (y_1, y_2, \cdots, y_m)^T \tag{A7}$$

It is clear from Eq. (A4) that the weigh vector $\boldsymbol{w}$ can be obtained by the matrix inversion. The following

simple estimate is adopted to determine the width in Eq. (A2) [23]:

$$r_j = \frac{d_{j,\max}}{\sqrt{n}\sqrt[n]{m-1}} \quad j = 1, 2, \cdots, m \tag{A8}$$

where n denotes the number of design variables, m the number of sampling points, $d_{j,\max}$ the maximum distance between the j-th sampling point and another one in the sampling points.

Density function to find an unexplored region

In the SAO, it is important to find out the unexplored region for global approximation. In order to find out the unexplored region with the RBF network, we have developed a function called the density function [23]. The procedure to construct the density function is summarized as follows:

(D-STEP1) The following vector $\boldsymbol{y}^D$ is prepared at the sampling points.

$$\boldsymbol{y}^D = (1, 1, \cdots, 1)^T_{m\times 1} \tag{A9}$$

(D-STEP2) The weight vector $\boldsymbol{w}^D$ of the density function $D(\boldsymbol{x})$ is calculated as follows:

$$\boldsymbol{w}^D = \left(\boldsymbol{H}^T\boldsymbol{H} + \boldsymbol{\Lambda}\right)^{-1}\boldsymbol{H}^T\boldsymbol{y}^D \tag{A10}$$

(D-STEP3) The density function $D(\boldsymbol{x})$ is minimized.

$$D(\boldsymbol{x}) = \sum_{j=1}^{m} w_j^D K(\boldsymbol{x}, \boldsymbol{x}_j) \rightarrow \min \tag{A11}$$

(D-STEP4) The point minimizing $D(\boldsymbol{x})$ is taken as the new sampling point.

Figure 18 shows an illustrative example in one dimension. The black dots denote the sampling points. It is found from Fig. 18 that local minima are generated around the unexplored region. The RBF network is basically the interpolation between sampling points: therefore, points A and B in Fig. 18 are the lower and upper bounds of the design variables of the density function.

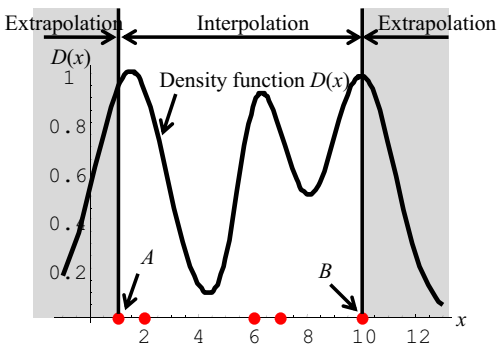

Fig. 18 Illustrative example of density function in one dimension

References

1. Obermeyer EJ, Majlessi SA (1998) A review of recent advances in the application of blank-holder force towards improving the forming limits of sheet metal parts. J Mater Process Technol 75: 222–234
2. Hsu CW, Ulsoy AG, Demeri MY (2000) An approach for modeling sheet metal forming for process controller design. J Manuf Sci Eng 122:717–724
3. Manabe K, Koyama H, Yoshihara S, Yagami T (2002) Development of a combination punch speed and blank-holder fuzzy control system for the deep-drawing process. J Mater Process Technol 125-126:440–445
4. Sheng ZQ, Jirathearanat S, Altan T (2004) Adaptive FEM simulation for prediction of variable blank holder force in conical cup drawing. International Journal of Machine Tools & Manufacturing 44:487–493
5. Lo SW, Yang TC (2004) Closed-loop control of the blank holding force in sheet metal forming with a new embedded-type displacement sensor. Int J Adv Manuf Technol 24:553–559
6. Lin ZQ, Wang WR, Chen GL (2007) A new strategy to optimize variable blank holder force towards improving the forming limits of aluminum sheet metal forming. J Mater Process Technol 183:339–346
7. Yagami T, Manabe K, Yamauchi Y (2007) Effect of alternating blank holder motion of drawing and wrinkle elimination on deep-drawability. J Mater Process Technol 187-188:187–191
8. Kitayama S, Hamano S, Yamazaki K, Kubo T, Nishikawa H, Kinoshita H (2010) A closed-loop type algorithm for determination of variable blank holder force trajectory and its application to square cup deep drawing. Int J Adv Manuf Technol 51:507–571
9. Wang WR, Chen GL, Lin ZQ, Li SH (2007) Determination of optimal blank holder force trajectories for segmented binders of step rectangle box using PID closed-loop FEM simulation. Int J Adv Manuf Technol 32:1074–1082
10. Jakumeit J, Herdy M, Nitsche M (2005) Parameter optimization of the sheet metal forming process using an iterative parallel Kriging algorithm. Struct Multidiscip Optim 29:498–507
11. Wang H, Li G, Yao Z, Zhi H (2008) Optimization of sheet metal forming processes by adaptive response surface based on intelligent sampling method. J Mater Process Technol 197:77–88
12. Kitayama S, Kita K, Yamazaki K (2012) Optimization of variable blank holder force trajectory by sequential approximate optimization with RBF network. J Adv Manuf Technol 61(9–12):1067–1083
13. Kitayama S, Huang S, Yamazaki K (2013) Optimization of variable blank holder force trajectory for springback reduction via sequential approximate optimization with radial basis function network. Struct Multidiscip Optim 47(2):289–300
14. Park SH, Yoon JH, Yang DY, Kim YH (1999) Optimum blank design in sheet metal forming by the deformation path iteration method. International Journal of Mechanical Science 41:1217–1232
15. Wang J, Goel A, Yang F, Gau JT (2009) Blank optimization for sheet metal forming using multi-step finite element simulations. Int J Adv Manuf Technol 40:709–720
16. Vafaeesefat A (2011) Finite element simulation for blank shape optimization in sheet metal forming. Mater Manuf Process 26:93–98
17. Fazli A, Arezoo B (2012) A comparison of numerical iteration based algorithms in blank optimization. Finite Elem Anal Des 50: 207–216
18. Oliveira MC, Padmanabhan R, Baptista AJ, Alves JL, Menezes LF (2009) Sensitivity study on some parameters in blank design. Mater Des 30:1223–1230

19. Hino R, Yoshida F, Toropov VV (2006) Optimum blank design for sheet metal forming based on the interaction of high- and low-fidelity FE models. Arch Appl Mech 75(10):679–691
20. Naceur H, Ben-Elechi S, Batoz JL, Knopf-Lenoir C (2008) Response surface methodology for the rapid design of aluminum sheet metal forming parameters. Mater Des 29:781–790
21. Liu Y, Chen W, Ding L, Wang X (2013) Response surface methodology based on support vector regression for polygon blank shape optimization design. Int J Adv Manuf Technol 66:1397–1405
22. Meng D, Zhao S, Li L, Liu C A servo-motor driven active blank holder control system for deep drawing process. Int J Adv Manuf Technol. doi:10.1007/s00170-016-8723-0
23. Kitayama S, Arakawa M, Yamazaki K (2011) Sequential approximate optimization using radial basis function network for engineering optimization. Optim Eng 12(4):535–557
24. Hillmann, M., Kubli, W., (1999), Optimization of sheet metal forming processes using simulation programs, in: *Numisheet* '99, Beasnc, France, 1: 287–292.
25. Manoochehri M, Kolahan F (2014) Integration of artificial neural network and simulated annealing algorithm to optimize deep drawing process. Int J Adv Manuf Technol 73:241–249
26. Hosseini A, Kadkhodayan M (2014) A hybrid NN-FE approach to adjust blank holder gap over punch stroke in deep drawing process. Int J Adv Manuf Technol 71:337–355
27. Meng D, Zhao S, Li L, Liu C (2016) A servo-motor driven active blank holder control system for deep drawing process. Int J Adv Manuf Technol 87:3185–3193
28. Kitayama S, Natsume S, Yamazaki K, Han J, Uchida H (2016) Numerical investigation and optimization of pulsating and variable blank holder force for identification of formability window for deep drawing of cylindrical cup. Int J Adv Manuf Technol 82:583–593
29. Mostafapour A, Akbari A, Nakhaei MR Application of response surface methodology for optimization of pulsating blank holder parameters in deep drawing process of Al 1050 rectangular parts. Int J Adv Manuf Technol. doi:10.1007/s00170-016-9781-z
30. Ozturk E, Turkoz M, Halkaci HS, Koc M Determination of optimal loading profiles in hydromechanical deep drawing process using integrated adaptive finite element analysis and fuzzy control approach. Int J Adv Manuf Technol. doi:10.1007/s00170-016-8912-x
31. Xiao Y, Zhang H, Jiang Z (2016) An approach for blank dimension design considering energy consumption. Int J Adv Manuf Technol 87:1229–1235